Deciphering the effects of 2D/3D urban morphology on diurnal cooling efficiency of urban green space

Wanben Wu[1,2,3*], Fengxiang Guo[3], Sebastian Elze[3], Julius Knopp[3], Ellen Banzhaf[3]

[1]Center for Ecological Dynamics in a Novel Biosphere (ECONOVO), Department of Biology, Aarhus University, Vennelyst Blvd. 9, 8000, Aarhus, Denmark
[2]Ministry of Education Key Laboratory for Biodiversity Science and Ecological Engineering, National Observations and Research Station for Wetland Ecosystems of the Yangtze Estuary, and Shanghai Institute of EcoChongming (SIEC), Fudan University, Shanghai 200433, China
[3]UFZ-Helmholtz Centre for Environmental Research, Department Urban and Environmental Sociology, Permoserstr. 15, 04318 Leipzig, Germany

Abstract: Urban green spaces (UGS) have emerged as a main nature-based solution proven to effectively cool urban areas, and cooling efficiency (CE) serves as a prominent indicator for assessing the performance of UGS. Yet diurnal CE dynamics and the impact of 3D urban morphology remain underexplored. In this study, we employed diurnal land surface temperature (LST) data from Ecosystem Spaceborne Thermal Radiometer Experiment on Space Station (ECOSTRESS) to delve into the diurnal dynamics of the CE of UGS within the urban core area of Paris, France. Meanwhile, using high-resolution land cover data, digital height model, and explainable machine learning models, we elucidated the intricate relationship between various urban morphology metrics and CE during a 24-hour cycle. In summary, city-scale continuous monitoring revealed diurnal CE variations, with values ranging from 0.008 °C to 0.13 °C and a standard deviation of 0.04 °C. On an average of a day, the relative importance of the 2D and 3D urban form indicators was 77.25% and 22.75%, respectively. Enhancing the dispersion of trees or improving the integrity of non-tree vegetation patches proves to be an effective strategy for augmenting CE. The results can be further used in urban planning to improve urban thermal resilience and adaptability.

Keywords: Cooling efficiency, ECOSTRESS LST, Urban morphology metrics, Urban green space

Highlights

- We explore diurnal variations of cooling efficiency of urban green space in the megacity Paris.
- The relationship of cooling efficiency with urban forms varies across the day.
- The cooling efficiency is more influenced by the 2D urban form than the 3D counterpart.
- Taller trees had higher CEs, while more varied tree heights led to smaller CEs.

1. Introduction

Urban heat island (UHI) is a phenomenon in which urban areas have higher air and surface temperatures than surrounding non-urban areas (Oke 1988; Rizwan et al. 2008; Voogt and Oke 2003). UHI has an adverse effect on society, economy, and ecology (Akbari et al. 1996; Battles and Kolbe 2019; Herbel et al. 2018; Youngsteadt et al. 2015). It also detrimentally affecting the physical and mental well-being of its residents of citizens (Araujo et al. 2015; Robine et al. 2008; Rydin et al. 2012). Against the backdrop of global warming and rapid urbanization, the heightened occurrence of extreme heat events has emerged as a primary concern in urban areas (Habeeb et al. 2015; Tuholske et al. 2021). According to the World Health Organization, 166,000 people died from heat stress between 2000 and 2017 globally, and the number of people exposed to heat waves increased by 125 million between 2000 and 2016 (Howard and Krishna 2022). Consequently, addressing the mitigation of UHI has become an important focus in the realm of urban resilient development and research on urban sustainability (Akbari et al. 2016; Mohajerani et al. 2017; Wong et al. 2021).

Urban green space (UGS), recognized as nature-based solutions (Seddon et al. 2020), have been demonstrated as effective means to lower urban temperatures through the processes of evapotranspiration and shading (Akbari et al. 2016; Marando et al. 2022; Seddon et al. 2020). Cooling efficiency (CE), defined as the degree of temperature decrease resulting from a one-unit increase in vegetation abundance (such as a 1% increase in the extent of UGS) has been widely used to evaluate the function of UGS cooling functions (Cheng et al. 2023; Zhou et al. 2017). CE variations can arise from disparities in social and ecological context (Myint et al. 2015; Wang et al. 2020; Zhou et al. 2017). For instance, cities situated in hot and arid biomes exhibit higher CE values when contrasted with cities in hot and humid environments (Myint et al. 2015; Wang et al. 2020; Zhou et al. 2017). Furthermore, CE values can also vary across seasons (Zhou et al. 2017), different vegetation types (Pataki et al. 2011), and varying elevations (Zhao et al. 2014). However, how CE varies during a 24-hour cycle remains largely unexplored.

This gap can now be filled with the data from the Ecosystem Spaceborne Thermal Radiometer Experiment on Space Station (ECOSTRESS), a mission that commenced on June 29, 2018. It provides the highest spatial resolution (38m × 69m) thermal infrared data from space (Hulley et al. 2021). In contrast to polar satellites, ECOSTRESS can provide diurnal cycling of land surface temperature (LST) (Wang et al. 2023), and it has been widely used for urban thermal environmental research (Chang et al. 2021; Kamaraj et al. 2021; Vo and Hu 2021). For example, ECOSTRESS LST data was employed to investigate diurnal variations in LST and heat exposure in Xi'an, China across diverse local climate zones (Chang et al. 2021; Yuan et al. 2022) . In a parallel study, ECOSTRESS LST data was harnessed to evaluate and model diurnal temperature buffering in the forest restoration area (Hamberg et al. 2022).

Comprehending the impact of intricate urban morphology on the spatial heterogeneity of the LST is pivotal in the context of mitigating the UHI effect (Berger et al. 2017; Guo et al. 2023; Huang and Wang 2019; Wu et al. 2022). Indeed, 2D urban morphology metrics, like UGS coverage and its proportion to impervious surface area, have been established as primary contributors to the spatial variability of LST (Henits et al. 2017; Kikon et al. 2016). Recent research has demonstrated that incorporating 3D urban morphology factors can enhance our explanatory power by up to 20% when assessing variations in UHI intensity (Wu et al. 2022). Among these 3D factors, building height and tree height stand out as significant determinants in delineating LST variations within urban environments (Berger et al. 2017; Guo et al. 2023; Yu et al. 2020). The above studies advance our comprehension of how urban morphology influences LST and the UHI effect. Nevertheless, the precise influence of 2D and 3D urban morphology on the diurnal CE of UGS remains unclear.

Here, we examined the diurnal fluctuations in CE during summertime in Paris, utilizing high-resolution LST data provided by ECOSTRESS. To unravel the connections between urban morphology and CE, we derived various 2D and 3D urban morphology metrics from high-resolution land cover data and detailed information on building and tree heights. Moreover, a more in-depth analysis was conducted to examine the varied impacts of distinct urban form characteristics on CE during different time intervals. Our investigation aimed to address the following two questions: (1) What are the spatiotemporal patterns of diurnal CE variations in the mega-city Paris Region? (2) How does urban morphology influence diurnal CE?

2. Study area and data collection

2.1 Study area

Paris, the capital of France, is a sprawling European megacity in Europe in the interior of the country with an area of 12,012 km^2 and a population of 12 million residents. Paris has received a great deal of attention for its UHI problem, especially since the 2003 heatwave event in Paris resulted in many losses (Fouillet et al. 2008). The urban boundary is defined as an essential property of cities, and the global urban boundary (GUB) product was generated based on 30m global artificial impervious area data (Gong et al. 2020; Li et al. 2020). Here we use GUB in 2015 to extract the urban core area of Paris, which is used as our study area. GUB data are accessible and can be downloaded from the website of https://data-starcloud.pcl.ac.cn/zh.

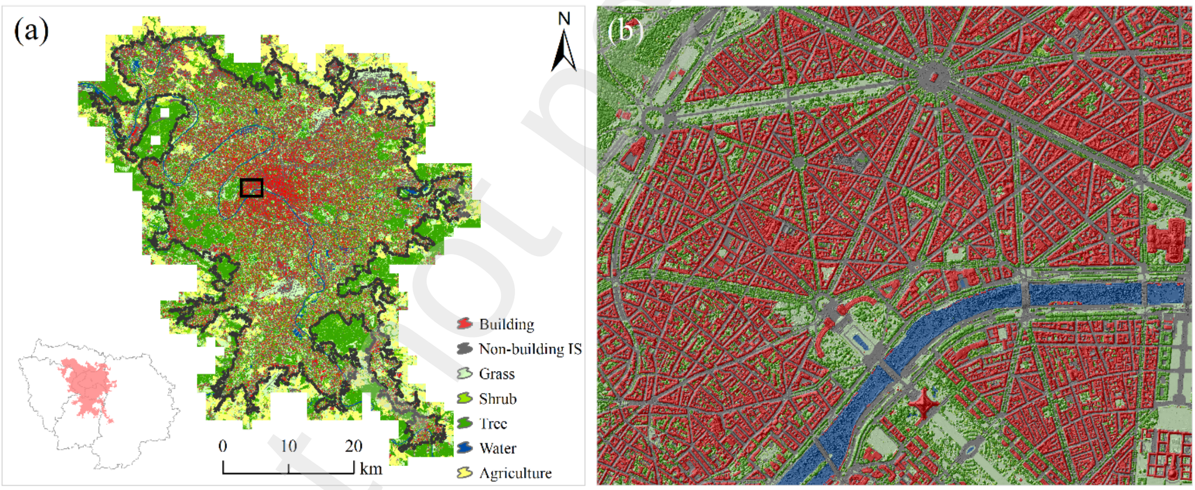

Fig.1. (a) Study area and land-cover map, where IS means imperious surface. (b) 3D urban information in a sample case.

2.2 Land cover data

The high-resolution land cover dataset utilized in this study originates from diverse existing products., including the MOS+ 2017-81 (IPR 2017), the green cadaster of the Department Hauts-de-Seine (DHS 2012), vegetation height (APUR 2017) and building footprints (IPR 2018), Copernicus Small and Woody features (Copernicus 2018a), and the Copernicus Street tree layer (Copernicus 2018b).

To accomplish this, data types were merged according to a ruleset, where priority is given to the highest resolution or thematic content. To reduce the number of thematic classes in the dataset, land- use and land-cover classes were harmonized and aggregated. The output was then rasterized to land cover map with seven types and 5 m resolution (Figure 1a). The identified categories cover building, non-building imperious surface (IS), grass, shrub, tree, water, and agricultural land cover.

2.3 Building and tree height

Building height and tree heights for the urban core area of Paris in 2015 were determined through the analysis of aerial photographs (Louis-Lucas et al. 2021), which were created by contrasting the Digital Surface Model (DSM) with the Digital Terrain Model (DTM). Both building footprint and tree height data are available on the website (https://opendata.apur.org/search), stored in raster format with a spatial resolution of 1m.

2.4 ECOSTRESS LST data

EOSTRESS LST data were obtained from ECOSTRESS Level-2 product, which is generated by a physic-based Temperature Emissivity Separation (TES) algorithm (Hook et al. 2019; Mira et al. 2007). ECOSTRESS LST has a repeating cycle every three to five days and a spatial resolution of 70m, which is resampled from the original pixel size (Xiao et al. 2021). Based on a global scale validation, ECOSTRESS LST has a high accuracy compared to ground-based observations with an overall root mean square error of 1.07K, mean absolute error of 0.4K and high r^2 (>0.988) (Hulley et al. 2021). Here we employed LST products from the warm summer months (June, July, August, September) from 2018 to 2023. Figure2 shows the diurnal LST patterns in the study area. All the cloud pixels were excluded using ECOSTRESS L2 cloud mask (ECO2CLD) product (Anderson et al. 2021). Meanwhile, the time of all data is converted to local time by adding 2 hours according to the time zone of Paris (UTC+2). The ECOSTRESS LST and ECO2CLOUD products used in this study can be freely accessed from the website of https://www.earthdata.nasa.gov/.

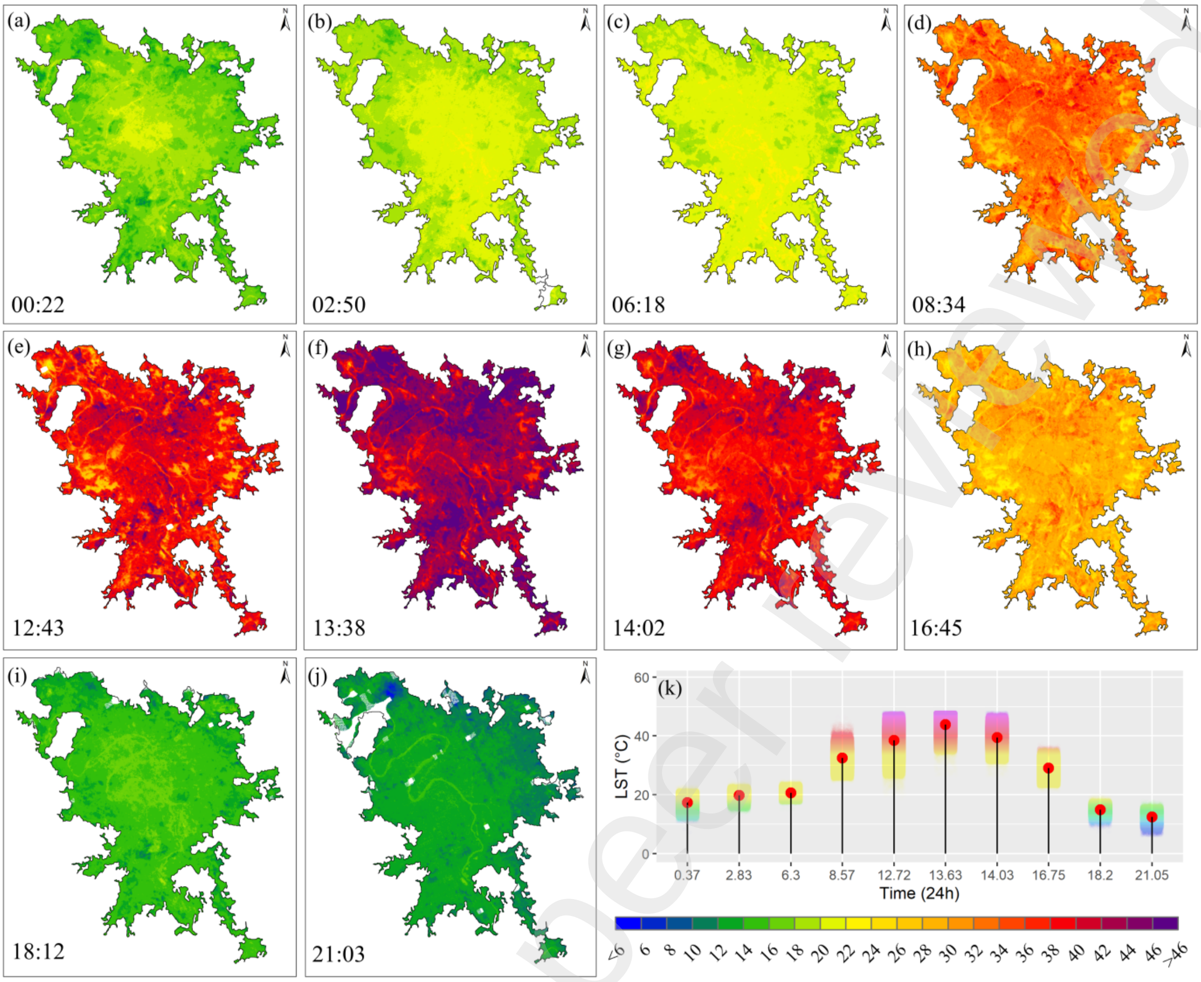

Fig.2. (a)-(j) Diurnal variations and spatial pattern of LST over the urban area of Paris Region, all times are CEST time (UTC+2). (k) Regional average LST for different time slots (in 24h) in the GUB region of Paris.

3. Method

3.1 Cooling efficiency calculation

According to the definition of CE, it signifies the reduction in temperature associated with a one-unit increase in vegetation abundance (e.g. 1% increase in UGS cover) (Wang et al. 2020; Zhou et al. 2017). The calculation of CE can be performed using the following equation. In this study, the urban green space coverage (UGSC) is defined as the total area covered by various types of vegetation, encompassing trees, shrublands, and grasslands. To elucidate the dynamics of CE at the city scale and discern the spatial nuances of CE, assessments were conducted at both city and grid scales using the Ordinary Least Squares (OLS) linear regression. At the city scale, UGSC and average LST were computed for each 840 m × 840 m grid and CE are conducted based on OLS linear regression. For the CE at grid-scale, the UGSC calculations were conducted for each 70m grid, with CE computed for each 840 m × 840 m grid.

$$CE = -\frac{\Delta LST}{\Delta UGSC}$$

3.2 Urban morphology metrics

To elucidate the influence of urban morphology metrics on CE, this study employs a diverse suite of urban morphology metrics. For 2D metrics, a nuanced consideration of patch density, edge density, largest patch index, landscape shape index, and percentage of patch type are undertaken across various land cover categories. The analysis encompasses four distinct land cover types: building, non-building impervious surface (IS), tree, and non-tree vegetation, leading to the inclusion of a comprehensive set of 20 unique 2D metrics. Concurrently, the investigation extends to the realm of 3D metrics, where 17 distinct metrics are derived from building and tree height information. These encompass fundamental measures such as the mean and standard deviation of height, along with an array of metrics characterizing diverse aspects of building forms, including largest patch index based and landscape shape index based on building surface area, etc. Table 1 shows how all metrics are calculated and defined. The computation of all 2D landscape metrics is executed through the utilization of the "landscapemetrics" package (Hesselbarth et al. 2019) in R (version 4.0.2). This computational process is conducted on an 840 m × 840 m grid size. Furthermore, the extraction of building landscape metrics in 3D space is facilitated through the application of the LPA3D software (Guo et al. 2022).

Table1. 2D and 3D urban morphology metrics

Urban forms	Metrics	Abb.	Description
2D	Patch density	PD	the ratio between number of patches to the areas, it describes the fragmentation of the landscape.
	Edge density	ED	all edges in the landscape in relation to the landscape area.
	Largest patch index	LPI	the percentage of the landscape covered by corresponding largest patch of each class.
	Landscape shape index	LSI	the ratio between the actual landscape edge length and the hypothetical minimum edge length.
	Percentage of patch type	PLAND	percentage of the landscape belonging to class i.
3D	Sub-high building coverage	Sub-high_BC	area percentage of subhigh-rise buildings (30m-100m).
	Middle building coverage	Middle_BC	area percentage of middle-rise buildings (20m-30m).
	Sub-low building coverage	Sub-low_BC	area percentage of sublow-rise buildings (10m-20m).
	Low building coverage	Low_BC	area percentage of low-rise buildings (below 10m).
	Building Shade metrics	CNI	the ratio between building height and building spacing.
	Landscape division index	LDI	aggregation degree of buildings. LDI =0 when the landscape consists of single patch.
	Largest patch index	LPI	largest space occupation of single building.
	Landscape shape index	LSI	deviation between patch shape and regular circle or square with same.
	Proximity index	PROX	the ratio between building height and square of building spacing.
	Surface area	SA	surface fluctuation compared with plane area.

Surface developed ratio	SDR	deviation of building surface to projected plane.
Building surface slope	SSL	integral slope of building surface, which is the sum of surface fluctuation at adjacent building pixels.
Mean Volume index	VOL	mean volume of buildings.
Mean building height	BH	mean height of the buildings.
Standard deviation of building height	BH_Std	undulation of the urban buildings surface.
Mean tree height	TH	average tree height.
Standard deviation of tree height	TH_Std	undulation of the tree canopy.

3.3 Statistical analysis

The boosted regression tree (BRT) model has been widely employed for investigating intricate and non-linear relationships between variables due to its capacity to mitigate the risk of overfitting (Friedman 2002). Here, a series of BRT models was utilized to assess the relative importance of various urban metrics on CE across different time intervals. Metrics exhibiting a substantial relative importance value are indicative of their primary role in depicting the spatial variability of CE. The BRT models were fitted using the gbm.step function within the "dismo" package (Elith and Leathwick 2017) in R (version 4.0.2). The four BRT parameters, learning rate, tree complexity, number of trees, and bag fraction, were set at 0.001, 5, 1000, and 0.75, respectively.

To examine the relationship between 2D/3D urban morphology metrics and diurnal CE, a series of generalized linear models (GLM) were constructed. Employing Akaike's Information Criterion corrected (AICc) through an information-theoretic approach, the best-fitting GLM model was determined based on the smallest AICc value. The correlation coefficient was utilized to gain further insights into the relationship between various urban morphology metrics and CE. Specifically, negative coefficients signify that a specific indicator is linked to a reduction in CE values. Conversely, positive coefficients indicate that an escalation in the indicator's value is correlated with an increase in CE values. Notably, only relationships deemed statistically significant (p-value < 0.05) were considered in this study.

4. Result

4.1 Diurnal CE in city scale

As expected, the CE shows obvious diurnal variation, Fig.3 depicts the intricate association between UGSC and CE across an 840m × 840m grid on a city scale. The statistical analysis reveals a significant correlation between UGSC and LST (p-value < 0.05). On this scale, continuous monitoring exhibited a range of CE values from 0.008 ℃ (21:03) to 0.13 ℃ (12:43), showcasing a mean of 0.059 ℃ and a standard deviation of 0.04 ℃. Concurrently, the coefficient of determination (R^2) exhibited a range from 0.013 (21:03) to 0.46 (08:34), illustrating a mean of 0.25 with a standard deviation of 0.15. Remarkably, this implies that up to 46% of the variations in LST can be elucidated by UGSC in urban areas. Examining the diurnal dynamic pattern, CE demonstrates an upward trajectory from the late-night hours (00:22) to the peak at midday (12:43), registering a maximum value of 0.13 ℃, followed by a declining trend in the afternoon and evening hours. Similarly, the diurnal pattern of R^2 mirrors this trend, with the highest R^2 occurring at 08:34 (0.46).

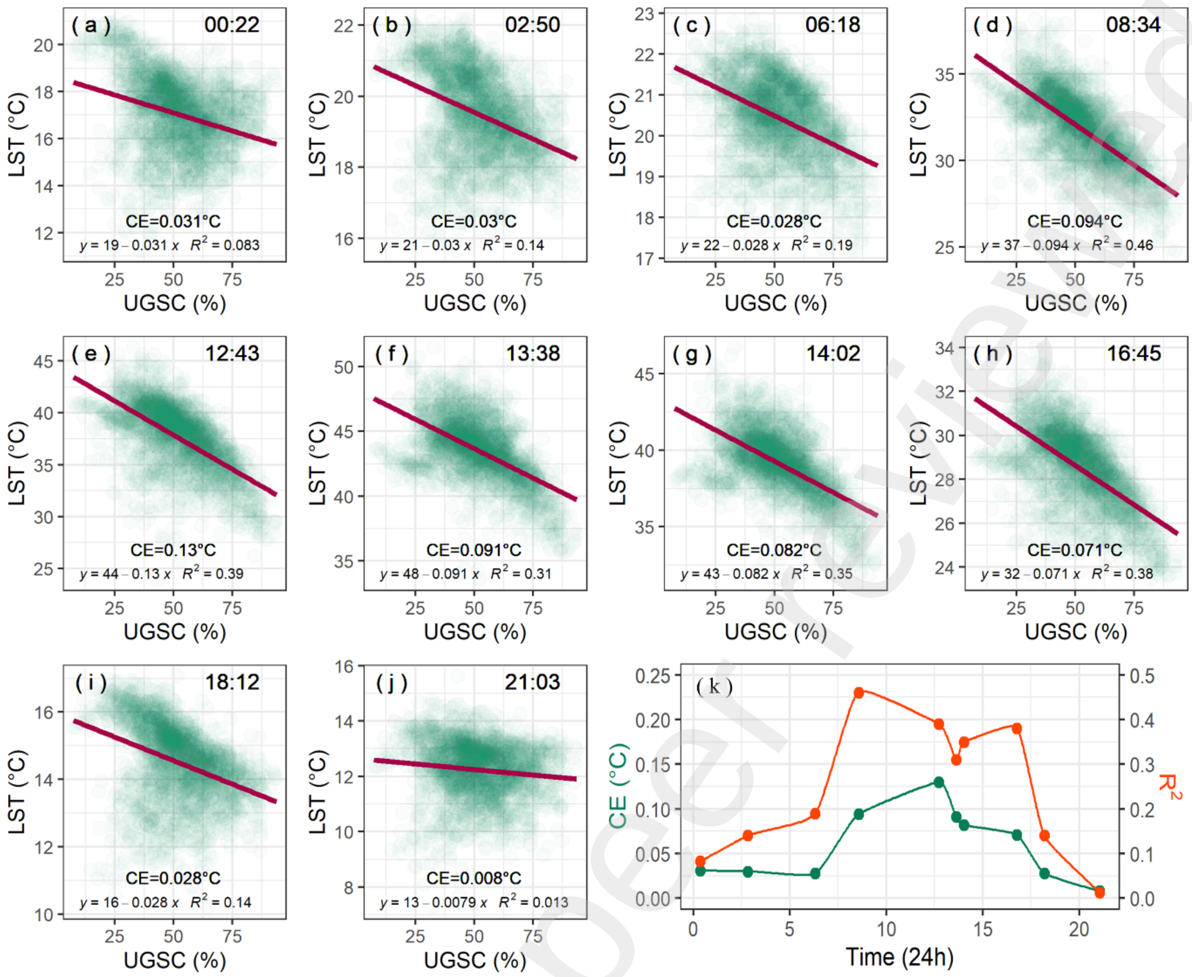

Fig.3. (a)-(j) Scatter plots of the relationship between UGSC and LST at different times and the fitted line based on the OLS linear regression model, each point represents the average of the LST in an 840m grid cell and the coverage of the UGS in that grid. (k) is the time series of CE values and model R^2 at the city scale.

4.2 Diurnal CE in grid scale

The diurnal variation of CE exhibits dynamic patterns at different times. During nighttime intervals such as 00:22, 02:50, and 21:03 (see Fig. 4a, b, j), substantial portions of the area, particularly in the core city center, manifest negative CE values. Interestingly, in the late afternoon, specifically at 18:12 (Fig. 4i), a sizable area in the city center also reveals negative CE values. Contrastingly, for daytime periods (Fig. 4c-h), most of the region registers positive CE values. Notably, parks and forested areas exhibit significantly higher CE values compared to densely built-up areas. The cumulative analysis (Fig. 4k) underscores that, on average, the mean CE predominantly assumes positive values throughout the study area, with discernibly elevated CE levels in the sub-core urban regions. Table 2 presents the statistical outcomes of diurnal CE corresponding to distinct time intervals. The highest CE value during day and night in 840m × 840m grid was 0.613 ℃ (13:38). At 12:43, the highest mean CE value of 0.038 ℃ was observed, coupled with the maximum standard deviation value of 0.035 ℃. Conversely, the minimum CE value of 0.0005 ℃ occurred at 21:03. In terms of the proportion of the area exhibiting positive CE values, the urban core area of the study demonstrated values ranging from 72.6% to 93.7% at daytime. Notably, at both 21:03 and 00:22, over 40% of the area exhibited negative CE values. On average, the mean CE value across all time intervals was calculated to be 0.016 ℃, accompanied by a standard deviation of 0.012 ℃. Remarkably, 94.5% of the urban core area in Paris Region exhibited positive average CE values.

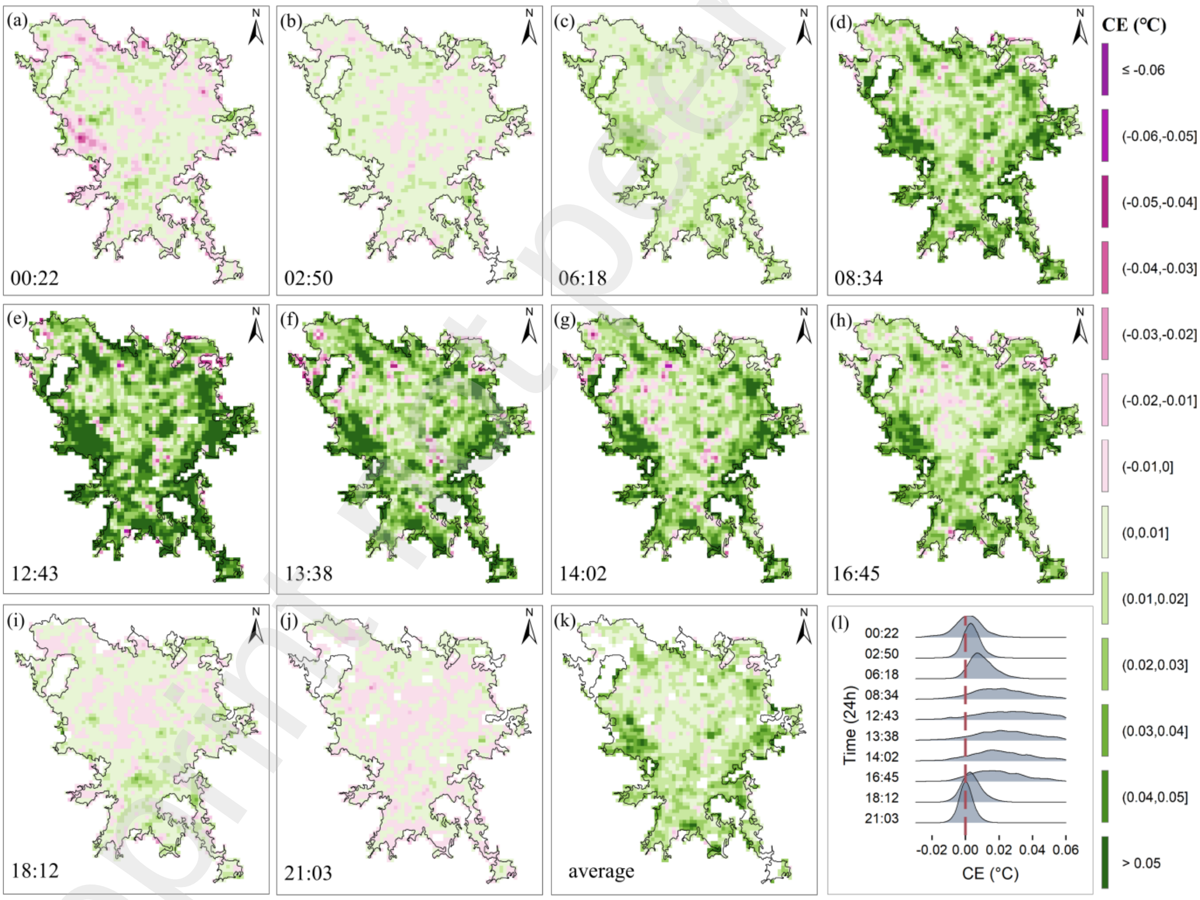

Fig.4. The diurnal variations and spatial pattern of CE over Paris with a resolution of 840m. (a)-(j) illustrate the diurnal variations of CE at different times of the day. (k) shows the average CE over time,

while (l) presents the distribution of CE values for different times. The red dashed line indicates a CE value of 0.

Table2. Statistics of CE (℃) at different observation times as presented in this study, where SD represent standard deviation of CE values.

times	Daytime/nighttime	Max	Min	Mean	SD	Fraction (CE>0)
00:22	Nighttime	0.044	-0.045	0.001	0.009	58.6%
02:50	Nighttime	0.052	-0.025	0.004	0.005	78.2%
06:18	Daytime	0.042	-0.011	0.01	0.007	93.7%
08:34	Daytime	0.231	-0.041	0.023	0.02	91.4%
12:43	Daytime	0.405	-0.053	0.038	0.035	91.5%
13:38	Daytime	0.613	-0.068	0.029	0.029	90.5%
14:02	Daytime	0.423	-0.055	0.024	0.024	88.8%
16:45	Daytime	0.104	-0.034	0.02	0.017	90.2%
18:12	Daytime	0.042	-0.095	0.004	0.007	72.6%
21:03	Nighttime	0.024	-0.022	0.0005	0.004	52.6%
Average	-	0.082	-0.014	0.016	0.012	94.5%

4.3 Relative importance or urban morphology metrics for CE

Fig. 5 presents an assessment of the relative importance of the different urban morphology metrics in influencing diurnal CE. On average, the top five influential urban morphology metrics are tree coverage (22.3%), tree largest patch index (19.3%), non-tree coverage (9.6%), tree height (7%), and tree edge density (4.4%). Notably, at 6:18, tree coverage exhibits the highest relative importance value, reaching 49.6%. The pivotal role of 2D and 3D urban morphology metrics in influencing CE is underscored in Fig. 6, where, on average, the relative importance of 2D and 3D urban morphology metrics are 77.25% and 22.75%, respectively. To the relative importance of CE across the entire day. The cumulative impact of 2D and 3D urban morphology metrics on CE varies temporally. Specifically, 2D metrics assume heightened importance at 13:38, reaching 86.6%, whereas 3D metrics peak at 00:22, constituting 39.94% of the total relative importance.

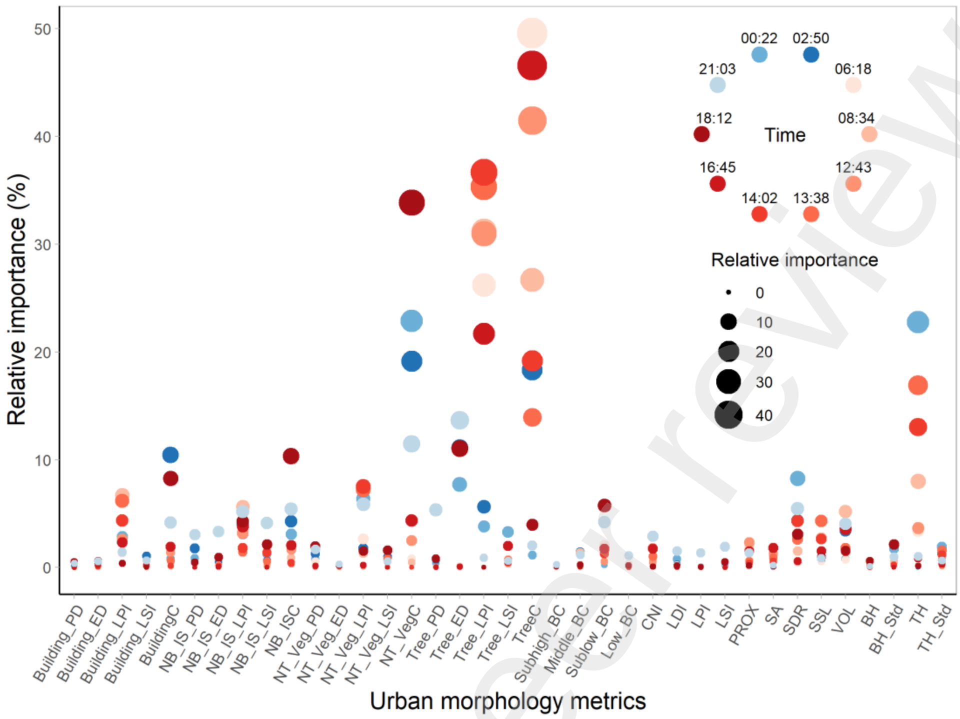

Fig.5. Relative importance of urban morphology metrics on diurnal CE.

Fig.6. Relative importance changes of 2D and 3D urban morphology metrics in the day.

4.4 Relationships between urban morphology metrics and CE

To enhance our comprehension of the intricate relationship between CE and diverse urban morphology metrics, we employed a series of GLM regression analyses encompassing 37 urban morphology metrics. Figure 7 illustrates the regression coefficients elucidating the associations between urban morphology metrics and diurnal CE.

In the realm of 2D urban morphology metrics, both land cover composition and configuration exert substantial influence on diurnal CE. Robust associations were observed, particularly in relation to building coverage and vegetation coverage. Notably, during daytime hours, UGS exhibit heightened cooling efficiency in areas characterized by elevated building coverage, contrasting with the nighttime scenario. Regarding vegetation cover, a conspicuous positive correlation is evident between CE and both non-tree vegetation and tree coverage during day and night. Land cover configuration metrics also manifest notable effects on diurnal CE. For instance, an increase in the LSI of impervious surfaces during the daytime was found to be associated with a decrease in CE. The relationship between CE and LSI exhibited variations between trees and non-tree vegetation. Specifically, heightened shape complexity of non-tree vegetation significantly increased CE, whereas the LSI of tree patches showed a significant negative correlation with CE as does non-treen vegetation patch density. Simultaneously, tree patch density demonstrated a significant positive relationship with CE.

For 3D urban morphology metrics, CE values increase as low-rise building coverage increases during daytime. The SA shows a negative correlation with CE both during day and night, while the SDR exhibits a negative correlation with CE during the day but a positive correlation at night. SSL is positively correlated with CE during the day but negatively correlated at night. The imagery of CE is influenced similarly by building height and tree height, during the day, both tall buildings and tall trees contribute to increased CE values. However, higher heterogeneity in building and tree heights results in smaller CE values.

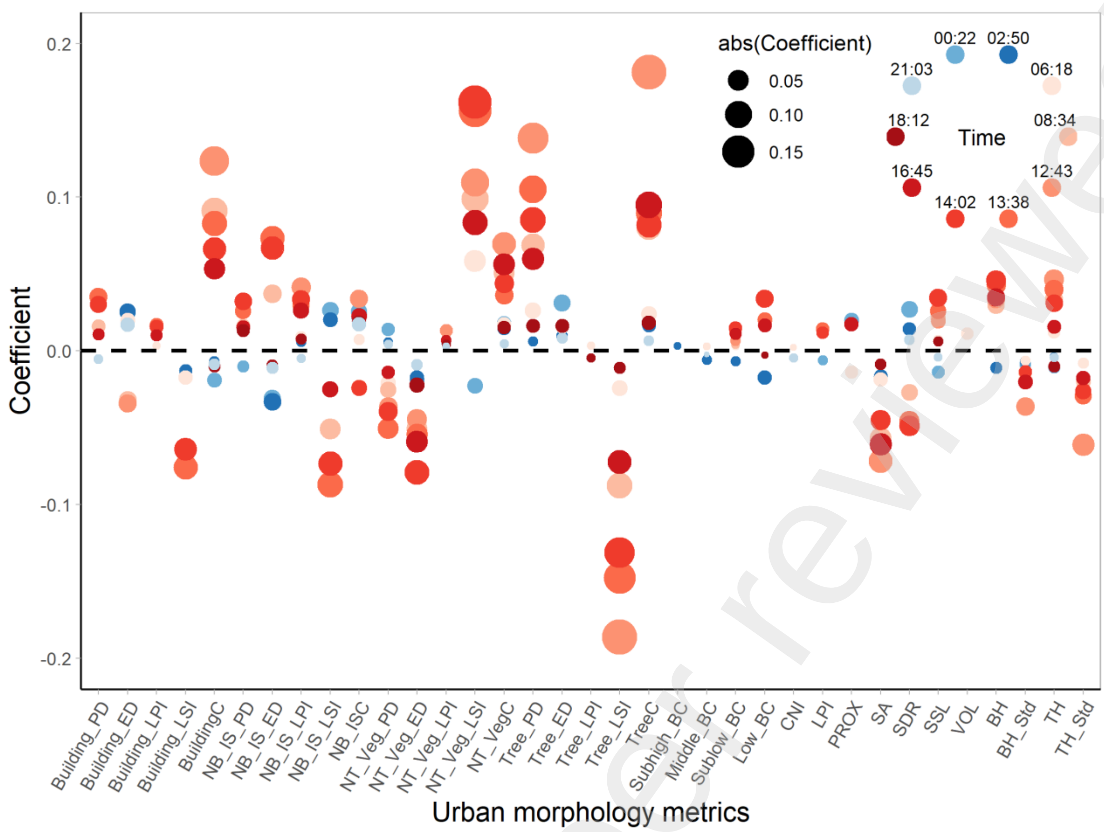

Fig7. Coefficients of various urban morphology metrics based on a series of GLM regression models. Only model results that pass the significance test (p-value<0.05) are shown here.

To further understand the image of LST for CE, Figure 8 shows the scatterplot distribution of LST vs. CE. The results show that there is a nonlinear relationship between LST and CE, which is manifested by the fact that when the temperature is lower than a certain threshold, the higher the temperature is, the larger the value of CE is, but when LST is higher than a certain value, the value of CE decreases as the temperature becomes higher. Based on the change-points estimation (with possibly random effects) algorithm (Muggeo and Muggeo 2017), the threshold value of LST can be estimated as 36.15℃.

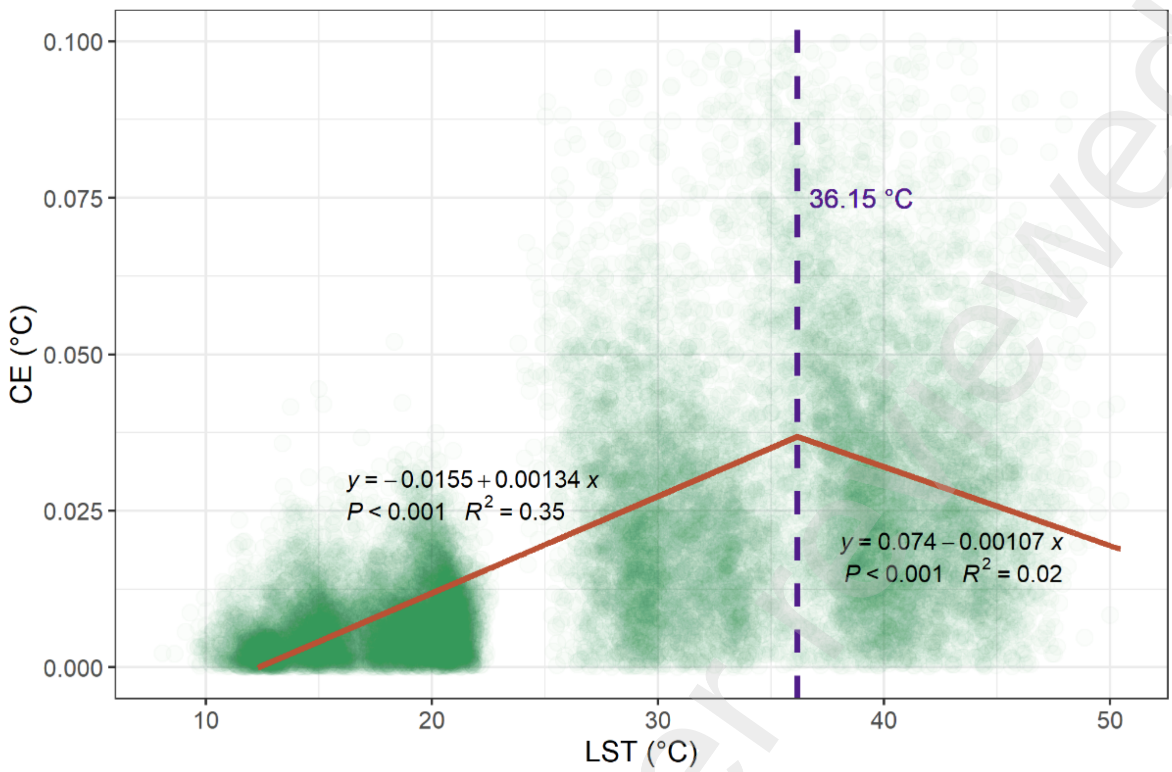

Fig.8. Relationship between LST and CE. The green point represents the mean LST and CE in an 840m grid. The purple dotted line indicates the turning point of LST change when CE starts a new trend. The turning point was extracted using the 'segmented' package (Muggeo and Muggeo 2017) in R (version 4.02). The red line represents the linear fitted relationship in the two stages.

5. Discussion

5.1 Diurnal dynamics of CE

By means of using the ECOSTRESS LST, the study showed how CE changes throughout the day and explored the influence of 2D and 3D urban structures. Unlike traditional analysis based on polar orbiting satellites thermal data like from Landsat (Kong et al. 2014), ASTER (Myint et al. 2015), and MODIS (Yang et al. 2022), ECOSTRESS LST allows us to examine UGS cooling abilities throughout the entire day because it's unfixed observation time (Hulley et al. 2019). By focusing on the Paris region, our case study showcases ECOSTRESS LST's effectiveness in revealing the spatial patterns of CE during a 24-hour cycle. Our findings enhance our understanding of intra-city urban heat dynamics and highlight the role of UGS in cooling the city during over the course of day and night. CE varies greatly over the course, ranging from 0.008 °C to 0.13 °C in the city scale, this is consistent with previous studies (0.023°C to 0.318°C) (Wang et al. 2020; Yang et al. 2022). There was a large difference between daytime and nighttime CE, with nighttime CE being smaller compared to daytime, possibly due to the absence of transpiration and shading effects of vegetation at night.

In addition, unlike previous studies on the variation of CE at the regional scale (Kong et al. 2014; Wang et al. 2020). Based on refined temperature and land cover data, this study attempts to compute CE in a smaller grid scale (840 m) to better understand the spatial distribution as well as the diurnal variation characteristics of CE in a large city. The results demonstrated that CE is highly heterogeneous in both time and space, for example, the average CE value in one day has a standard deviation of 0.012°C. The spatial distribution of CE at different times (Figure 4) also indicates that the cooling benefit of UGS has a strong inequality in the spatial distribution, and the map of CE can provide an effective reference to minimize this inequality.

5.2 Significant effects of urban morphology on CE

Based on explainable machine learning model, we find out that both 2D and 3D urban morphology metrics have significant effects on the CE of UGS. Specifically, the 2D urban forms play a more important role compared to 3D urban forms, because the 2D urban heterogeneity, such as land cover composition, is the main cause of land surface temperature variations (Rahimi et al. 2021). Meanwhile, the relative importance of 2D and 3D urban morphology metrics on CE shows a significant diurnal variation, where especially the 3D urban morphology metrics increase their relative importance in the midday (13:38) and in the deep night (00:22). This could be attributed to the increased prominence of tree shadows at 13:38, as the three-dimensional structure of the building significantly amplifies the heterogeneity of thermal storage capacity during nighttime.

Buildings exert a pronounced influence on the cooling efficiency of urban green spaces. On one hand, areas with higher building coverage experience enhanced cooling efficiency of vegetation, possibly attributed to the elevated surface temperatures in densely built areas, enabling vegetation to yield more substantial cooling effects. However, it is noteworthy that the cooling impact of vegetation becomes subdued as temperatures reach a certain threshold (Figure 8), as illustrated in Figure 7 where the correlation coefficient between building coverage and cooling efficiency peaks at 12:43.

Although CE can be significantly improved by increasing UGS cover, there are differences in the effects of tree and non-tree vegetation patterns on cooling efficiency. For example, increasing patch density or edge density of tree patches can significantly improve CE. This was mainly because that increasing edge density has the potential to allow trees to provide greater shading on continuous impervious surfaces (Wu et al. 2022). In addition, it expands energy flow and exchange between UGS and their surroundings (Cadenasso et al. 2003). However, non-tree vegetation (e.g., grasses and shrubs) lacks a shading effect, so increasing its degree of fragmentation (high ED and PD) rather reduces its cooling effect.

5.3 Implications for urban heat island effect mitigation

By engaging in this research, urban planners can gain important perspectives that will help them in designing urban areas and managing UGS to effectively counteract the impacts of urbanization on UHI. Based on the results of this study, we proposed the following recommendations for improving CE of UGS.

(1) Increased shape complexity and irregularity of tree patches decreases the CE of UGS, but increased edge density and patch density improves the CE, so when constructing new tree, consider laying out trees in a decentralized manner, and, at the same time, pursuing regularity in the shapes of individual patches.

(2) In contrast to trees, increasing the shape irregularity and complexity of non-tree vegetation can effectively optimize CE, while increasing ED or PD of non-tree vegetation can lead to lower CE. Therefore, when constructing new vegetation, such as grass and shrubs, continuous, complete, and more complex forms should be introduced rather than fragmented regular UGS.

(3) Considering taller trees when selecting tree species and ensuring consistency of tree heights in patches can effectively optimize CE.

5.4 Limitations and future research directions

Limitations and uncertainties accompany this study. The ECOSTRESS LST data were acquired from different days, even though we filtered the data from summertime, but there still have uncertainties for diurnal variation of CE research. More investigations on the method for adjusting ECOSTRESS LST data may need to be conducted in the future. CE of UGS can be affected by many factors such as tree species, leaf size and color, climatic background of the region, and even anthropogenic heat emissions. More fieldwork and measurements of tree species and detailed climate records will support a better understanding of factors affecting CE. Meanwhile, a machine learning model can elucidate the intricate relationship between urban morphology and CE. However, it falls short in providing a comprehensive understanding of the complete trajectory of these influences. Future research endeavors could explore the incorporation of indicators such as shadows and evapotranspiration (ET) as interpermeates, aiming to deepen our comprehension of the intricate ways in which urban morphologies impact CE. In this study, a grid-based method was employed, yet it focused solely on a single scale. It is imperative to acknowledge that varying grid scales may yield divergent results (Guo et al. 2023). Consequently, the exploration of scale-effect phenomena should be prioritized in future investigations. Lastly, owing to the unavailability of spatial-temporal continent air temperature data, our assessment was confined to evaluating diurnal CE dynamics based on LST. The evaluation of spatial-temporal changes in canopy temperature-based CE holds significant value and should be a focal point in forthcoming studies.

6. Conclusions

The main objective of this study is to investigate the diurnal dynamics of CE and, subsequently, to explore the impact of urban form (both 2D and 3D) on CE. To achieve this objective, we utilize ECOSTRESS LST data, overcoming the limitations associated with polar-orbiting satellites (e.g., Landsat and MODIS) observed in previous studies. The ECOSTRESS LST data allows us to acquire diurnal LST information, enabling a detailed analysis of the diurnal CE patterns in the study area, here in the Paris Region. To better understand the relationship between urban form and CE, we constructed twenty 2D morphological indicators and seventeen 3D morphological indicators based on high-resolution land cover data and urban 3D morphological information (including building and tree height information). The relative importance and relevance of different urban morphological indicators for CE are analyzed using BRT and GLM models. The results reveal a pronounced heterogeneity of CE both temporally and spatially throughout the day. Additionally, the influence of urban structure on CE exhibits significant variations at different times of the day. Drawing from the study's outcomes, practical suggestions are presented to enhance the CE of UGS, with potential applications in real-world scenarios. This study marks the first analysis of the diurnal variation of CE and its correlation with the 2D and 3D morphology of the city, introducing a novel perspective to the study of the urban thermal environment. The insights gained from this research can be instrumental in optimizing the CE of UGS in urban areas, thereby mitigating the adverse effects of extreme heat and enhancing urban resilience.

Acknowledgments

This research was supported by the National Key Research and Development Project of China (grant no. 2021YFE0193100), European Union's Horizon 2020 research and innovation program through the REGREEN project (grant no. 821016).

Reference

Akbari, H., Cartalis, C., Kolokotsa, D., Muscio, A., Pisello, A.L., Rossi, F., Santamouris, M., Synnefa, A., Wong, N.H., & Zinzi, M. (2016). Local climate change and urban heat island mitigation techniques–the state of the art. *Journal of Civil Engineering and Management, 22*, 1-16

Akbari, H., Rosenfeld, A., Taha, H., & Gartland, L. (1996). Mitigation of summer urban heat islands to save electricity and smog. In, *76th Annual Meteorological Society Meeting, Atlanta, GA*

Anderson, M.C., Yang, Y., Xue, J., Knipper, K.R., Yang, Y., Gao, F., Hain, C.R., Kustas, W.P., Cawse-Nicholson, K., & Hulley, G. (2021). Interoperability of ECOSTRESS and Landsat for mapping evapotranspiration time series at sub-field scales. *Remote Sensing of Environment, 252*, 112189

APUR (2017). Hauteur vegetation 2015. In: APUR

Araujo, R.V., Albertini, M.R., Costa-da-Silva, A.L., Suesdek, L., Franceschi, N.C.S., Bastos, N.M., Katz, G., Cardoso, V.A., Castro, B.C., & Capurro, M.L. (2015). São Paulo urban heat islands have a higher incidence of dengue than other urban areas. *Brazilian Journal of Infectious Diseases, 19*, 146-155

Battles, A.C., & Kolbe, J.J. (2019). Miami heat: urban heat islands influence the thermal suitability of habitats for ectotherms. *Global change biology, 25*, 562-576

Berger, C., Rosentreter, J., Voltersen, M., Baumgart, C., Schmullius, C., & Hese, S. (2017). Spatio-temporal analysis of the relationship between 2D/3D urban site characteristics and land surface temperature. *Remote Sensing of Environment, 193*, 225-243

Cadenasso, M.L., Pickett, S.T., Weathers, K.C., & Jones, C.G. (2003). A framework for a theory of ecological boundaries. *BioScience, 53*, 750-758

Chang, Y., Xiao, J., Li, X., Middel, A., Zhang, Y., Gu, Z., Wu, Y., & He, S. (2021). Exploring diurnal thermal variations in urban local climate zones with ECOSTRESS land surface temperature data. *Remote Sensing of Environment, 263*, 112544

Cheng, X., Liu, Y., Dong, J., Corcoran, J., & Peng, J. (2023). Opposite climate impacts on urban green spaces' cooling efficiency around their coverage change thresholds in major African cities. *Sustainable Cities and Society, 88*, 104254

Copernicus (2018a). Small Woody Features 2018. In: European Environment Agency

Copernicus (2018b). Urban Atlas Street Tree Layer 2018. In: European Environment Agency

DHS (2012). Cadastre vert - Masses vertes. In: Department Hauts-de-Seine

Elith, J., & Leathwick, J. (2017). Boosted Regression Trees for ecological modeling. *R Documentation. Available online: https://cran. r-project. org/web/packages/dismo/vignettes/brt. pdf (accessed on 12 June 2011)*

Fouillet, A., Rey, G., Wagner, V., Laaidi, K., Empereur-Bissonnet, P., Le Tertre, A., Frayssinet, P., Bessemoulin, P., Laurent, F., & De Crouy-Chanel, P. (2008). Has the impact of heat waves on mortality changed in France since the European heat wave of summer 2003? A study of the 2006 heat wave. *International journal of epidemiology, 37*, 309-317

Friedman, J.H. (2002). Stochastic gradient boosting. *Computational statistics & data analysis, 38*, 367-378

Gong, P., Li, X., Wang, J., Bai, Y., Chen, B., Hu, T., Liu, X., Xu, B., Yang, J., & Zhang, W. (2020). Annual maps of global artificial impervious area (GAIA) between 1985 and 2018. *Remote Sensing of Environment, 236*, 111510

Guo, F., Schlink, U., Wu, W., Hu, D., & Sun, J. (2023). Scale-dependent and season-dependent impacts of 2D/3D building morphology on land surface temperature. *Sustainable Cities and Society, 97*, 104788

Guo, F., Schlink, U., Wu, W., & Mohamdeen, A. (2022). Differences in Urban Morphology between 77 Cities in China and Europe. *Remote Sensing, 14*, 5462

Habeeb, D., Vargo, J., & Stone, B. (2015). Rising heat wave trends in large US cities. *Natural Hazards, 76*, 1651-1665

Hamberg, L.J., Fisher, J.B., Ruppert, J.L., Tureček, J., Rosen, D.H., & James, P.M. (2022). Assessing and modeling diurnal temperature buffering and evapotranspiration dynamics in forest restoration using ECOSTRESS thermal imaging. *Remote Sensing of Environment, 280*, 113178

Henits, L., Mucsi, L., & Liska, C.M. (2017). Monitoring the changes in impervious surface ratio and urban heat island intensity between 1987 and 2011 in Szeged, Hungary. *Environmental monitoring and assessment, 189*, 1-13

Herbel, I., Croitoru, A.-E., Rus, A.V., Roşca, C.F., Harpa, G.V., Ciupertea, A.-F., & Rus, I. (2018). The impact of heat waves on surface urban heat island and local economy in Cluj-Napoca city, Romania. *Theoretical and applied climatology, 133*, 681-695

Hesselbarth, M.H., Sciaini, M., With, K.A., Wiegand, K., & Nowosad, J. (2019). landscapemetrics: an open-source R tool to calculate landscape metrics. *Ecography, 42*, 1648-1657

Hook, S.J., Cawse-Nicholson, K., Barsi, J., Radocinski, R., Hulley, G.C., Johnson, W.R., Rivera, G., & Markham, B. (2019). In-flight validation of the ECOSTRESS, Landsats 7 and 8 thermal infrared spectral channels using the Lake Tahoe CA/NV and Salton Sea CA automated validation sites. *IEEE Transactions on Geoscience and Remote Sensing, 58*, 1294-1302

Howard, S., & Krishna, G. (2022). How hot weather kills: the rising public health dangers of extreme heat. *bmj, 378*

Huang, X., & Wang, Y. (2019). Investigating the effects of 3D urban morphology on the surface urban heat island effect in urban functional zones by using high-resolution remote sensing data: A case study of Wuhan, Central China. *ISPRS Journal of Photogrammetry and Remote Sensing, 152*, 119-131

Hulley, G., Shivers, S., Wetherley, E., & Cudd, R. (2019). New ECOSTRESS and MODIS land surface temperature data reveal fine-scale heat vulnerability in cities: A case study for Los Angeles County, California. *Remote Sensing, 11*, 2136

Hulley, G.C., Göttsche, F.M., Rivera, G., Hook, S.J., Freepartner, R.J., Martin, M.A., Cawse-Nicholson, K., & Johnson, W.R. (2021). Validation and quality assessment of the ECOSTRESS level-2 land surface temperature and emissivity product. *IEEE Transactions on Geoscience and Remote Sensing, 60*, 1-23

IPR (2017). Mode d'occupation du sol (MOS) 2017 a 81 postes. In: L'Institut Paris Region

IPR (2018). Densibati 2018. In: L'Institut Paris Region

Kamaraj, N.P., Shekhar, S., Sivashankari, V., Balasubramani, K., & Prasad, K.A. (2021). Detecting heat-inducing urban built-up surface material with multi remote sensing datasets using reflectance and emission spectroscopy. *Remote Sensing of Environment, 264*, 112591

Kikon, N., Singh, P., Singh, S.K., & Vyas, A. (2016). Assessment of urban heat islands (UHI) of Noida City, India using multi-temporal satellite data. *Sustainable Cities and Society, 22*, 19-28

Kong, F., Yin, H., James, P., Hutyra, L.R., & He, H.S. (2014). Effects of spatial pattern of greenspace on urban cooling in a large metropolitan area of eastern China. *Landscape and Urban Planning, 128*, 35-47

Li, X., Gong, P., Zhou, Y., Wang, J., Bai, Y., Chen, B., Hu, T., Xiao, Y., Xu, B., & Yang, J. (2020). Mapping global urban boundaries from the global artificial impervious area (GAIA) data. *Environmental Research Letters, 15*, 094044

Louis-Lucas, T., Mayrand, F., Clergeau, P., & Machon, N. (2021). Remote sensing for assessing vegetated roofs with a new replicable method in Paris, France. *Journal of applied remote sensing, 15*, 014501-014501

Marando, F., Heris, M.P., Zulian, G., Udías, A., Mentaschi, L., Chrysoulakis, N., Parastatidis, D., & Maes, J. (2022). Urban heat island mitigation by green infrastructure in European Functional Urban Areas. *Sustainable Cities and Society, 77*, 103564

Mira, M., Valor, E., Boluda, R., Caselles, V., & Coll, C. (2007). Influence of soil water content on the thermal infrared emissivity of bare soils: Implication for land surface temperature determination. *Journal of Geophysical Research: Earth Surface, 112*

Mohajerani, A., Bakaric, J., & Jeffrey-Bailey, T. (2017). The urban heat island effect, its causes, and mitigation, with reference to the thermal properties of asphalt concrete. *Journal of environmental management, 197*, 522-538

Muggeo, V.M., & Muggeo, M.V.M. (2017). Package 'segmented'. *Biometrika, 58*, 516

Myint, S.W., Zheng, B., Talen, E., Fan, C., Kaplan, S., Middel, A., Smith, M., Huang, H.-P., & Brazel, A. (2015). Does the spatial arrangement of urban landscape matter? Examples of urban warming and cooling in Phoenix and Las Vegas. *Ecosystem Health and Sustainability, 1*, 1-15

Oke, T.R. (1988). The urban energy balance. *Progress in Physical geography, 12*, 471-508

Pataki, D.E., McCarthy, H.R., Litvak, E., & Pincetl, S. (2011). Transpiration of urban forests in the Los Angeles metropolitan area. *Ecological Applications, 21*, 661-677

Rahimi, E., Barghjelveh, S., & Dong, P. (2021). Quantifying how urban landscape heterogeneity affects land surface temperature at multiple scales. *Journal of Ecology and Environment, 45*, 1-13

Rizwan, A.M., Dennis, L.Y., & Chunho, L. (2008). A review on the generation, determination and mitigation of Urban Heat Island. *Journal of environmental sciences, 20*, 120-128

Robine, J.-M., Cheung, S.L.K., Le Roy, S., Van Oyen, H., Griffiths, C., Michel, J.-P., & Herrmann, F.R. (2008). Death toll exceeded 70,000 in Europe during the summer of 2003. *Comptes rendus biologies, 331*, 171-178

Rydin, Y., Bleahu, A., Davies, M., Dávila, J.D., Friel, S., De Grandis, G., Groce, N., Hallal, P.C., Hamilton, I., & Howden-Chapman, P. (2012). Shaping cities for health:

complexity and the planning of urban environments in the 21st century. *The lancet, 379*, 2079-2108

Seddon, N., Chausson, A., Berry, P., Girardin, C.A., Smith, A., & Turner, B. (2020). Understanding the value and limits of nature-based solutions to climate change and other global challenges. *Philosophical Transactions of the Royal Society B, 375*, 20190120

Tuholske, C., Caylor, K., Funk, C., Verdin, A., Sweeney, S., Grace, K., Peterson, P., & Evans, T. (2021). Global urban population exposure to extreme heat. *Proceedings of the National Academy of Sciences, 118*, e2024792118

Vo, T.T., & Hu, L. (2021). Diurnal evolution of urban tree temperature at a city scale. *Scientific Reports, 11*, 10491

Voogt, J.A., & Oke, T.R. (2003). Thermal remote sensing of urban climates. *Remote Sensing of Environment, 86*, 370-384

Wang, J., Zhou, W., Jiao, M., Zheng, Z., Ren, T., & Zhang, Q. (2020). Significant effects of ecological context on urban trees' cooling efficiency. *ISPRS Journal of Photogrammetry and Remote Sensing, 159*, 78-89

Wang, Q., Wang, X., Meng, Y., Zhou, Y., & Wang, H. (2023). Exploring the impact of urban features on the spatial variation of land surface temperature within the diurnal cycle. *Sustainable Cities and Society, 91*, 104432

Wong, N.H., Tan, C.L., Kolokotsa, D.D., & Takebayashi, H. (2021). Greenery as a mitigation and adaptation strategy to urban heat. *Nature Reviews Earth & Environment, 2*, 166-181

Wu, W.-B., Yu, Z.-W., Ma, J., & Zhao, B. (2022). Quantifying the influence of 2D and 3D urban morphology on the thermal environment across climatic zones. *Landscape and Urban Planning, 226*, 104499

Xiao, J., Fisher, J.B., Hashimoto, H., Ichii, K., & Parazoo, N.C. (2021). Emerging satellite observations for diurnal cycling of ecosystem processes. *Nature Plants, 7*, 877-887

Yang, Q., Huang, X., Tong, X., Xiao, C., Yang, J., Liu, Y., & Cao, Y. (2022). Global assessment of urban trees' cooling efficiency based on satellite observations. *Environmental Research Letters, 17*, 034029

Youngsteadt, E., Dale, A.G., Terando, A.J., Dunn, R.R., & Frank, S.D. (2015). Do cities simulate climate change? A comparison of herbivore response to urban and global warming. *Global change biology, 21*, 97-105

Yu, S., Chen, Z., Yu, B., Wang, L., Wu, B., Wu, J., & Zhao, F. (2020). Exploring the relationship between 2D/3D landscape pattern and land surface temperature based on explainable eXtreme Gradient Boosting tree: A case study of Shanghai, China. *Science of the Total Environment, 725*, 138229

Yuan, B., Zhou, L., Hu, F., & Zhang, Q. (2022). Diurnal dynamics of heat exposure in Xi'an: A perspective from local climate zone. *Building and Environment, 222*, 109400

Zhao, L., Lee, X., Smith, R.B., & Oleson, K. (2014). Strong contributions of local background climate to urban heat islands. *Nature, 511*, 216-219

Zhou, W., Wang, J., & Cadenasso, M.L. (2017). Effects of the spatial configuration of trees on urban heat mitigation: A comparative study. *Remote Sensing of Environment, 195*, 1-12